I&EC research
Industrial & Engineering Chemistry Research

Article

pubs.acs.org/IECR

Dimethyl Ether Carbonylation to Methyl Acetate over Nanosized Mordenites

Huifu Xue,[†] Xiumin Huang,[†] Evert Ditzel,[‡] Ensheng Zhan,[†] Meng Ma,[†] and Wenjie Shen*[,†]

[†]State Key Laboratory of Catalysis, Dalian Institute of Chemical Physics, Chinese Academy of Sciences, Dalian 116023, China
[‡]Hull Research and Technology Centre, BP Chemicals Limited, Hull HU12 8DS, U.K.

ABSTRACT: Nanosized mordenites were found to show significantly enhanced reaction efficiency in dimethyl ether (DME) carbonylation to methyl acetate (MA) because of a greatly facilitated diffusion process. Copper incorporation into the channels of the nanosized mordenites further promoted the reaction rate, selectivity, and stability. Moreover, upon the addition of a small amount of H_2 (5−19 vol %) to the feed gas, deactivation was suppressed during DME carbonylation, whereas the catalyst stability and rate of formation of MA increased.

1. INTRODUCTION

The carbonylation of dimethyl ether (DME) to methyl acetate (MA) over solid zeolites is a new route for transforming C1 compounds into C2 chemicals through C−C coupling,[1,2] and H-mordenite (HMOR) serves as the most active catalyst for this reaction by far.[1−11] Mechanistic and kinetic studies identified that DME carbonylation is initiated by the dissociative adsorption of DME on the Brønsted acid sites of the zeolites, forming CH_3* species, followed by the insertion of CO into the CH_3* species to produce an acetyl group (CH_3CO*). This crucial intermediate reacts with another DME molecule to form methyl acetate and regenerate the surface methoxy species.[1−3] Experimental and theoretical analyses have revealed that the size of the eight-membered-ring (8-MR) channels of HMOR and the unique orientation of the methoxy groups in the 8-MR channels are responsible for stabilizing the CH_3CO* intermediate, and thus, these factors account for the superior activity for DME carbonylation.[4,5,11] However, HMOR catalyst, similarly to most zeolites, suffers from severe deactivation due to the deposition of carbonaceous species during the course of the reaction. For example, the surface methoxy groups in the 12-membered-ring (12-MR) channels react more rapidly with DME to form a trimethyl oxonium cation (TMO^+) that can further aggregate into hydrocarbons and/or aromatics.[11] Therefore, suppressing coke formation in the 12-MR channels of HMOR to enhance the catalyst stability still remains challenging.

Nanosized zeolites have been found to greatly facilitate diffusion and, thereby, to dramatically suppress the coke deposition.[12] Reducing the crystalline size from the typical micrometer scale to the nanometer level shortens the diffusion pathway and improves the efficiency of molecule transportation. For example, decreasing the size of HZSM-5 to about 100 nm was found to markedly enhanced the catalytic stability in *n*-hexane cracking,[13,14] acetone to olefin,[15,16] methanol to gasoline,[17,18] and methanol to DME.[19] Nanosized Beta zeolites (80−100 nm) also exhibited activity and stability superior to those of the conventional zeolites with large particle sizes (2−4 μm) in acylation of anisole and toluene.[20] In this work, we examined nanosized HMOR for DME carbonylation with respect to the catalytic activity and stability. Compared to conventional HMOR,[9,10] nanosized mordenite provided a substantially enhanced reaction rate and long-term stability. Cu doping further promoted the overall reaction efficiency based on the crucial role of copper in activating CO and eliminating coke accumulation. Moreover, the addition of a small amount of H_2 (5−19 vol %) to the feed gas suppressed the accumulation of carbonaceous species and consequently prolonged the high catalytic performance.

2. EXPERIMENTAL SECTION

2.1. Synthesis of the HMOR Catalysts. The microsized mordenite (HMOR-C) was prepared from a commercial sample, following a typical ion-exchange procedure that we reported previously.[21]

The nanosized HMOR was prepared by a hydrothermal process.[22] In this case, 2.71 g of $Al(NO_3)_3{\cdot}3H_2O$ and 4.7 g of Et_6-diquat-5 (*N*,*N*,*N*,*N*′,*N*′,*N*′-hexaethylpentanediammonium cations) were dissolved in 60 mL of 1.0 M NaOH aqueous solution, and then 21.28 g of silica sol (30.6 wt % SiO_2 with a mean particle size of 10 nm) was added. The mixture was stirred at room temperature for 24 h and then transferred into a Teflon-lined autoclave (100 mL). After being crystallized at 433 K for 7 days under stirring, the solid product was filtrated, washed with water, dried at 383 K for 12 h, and finally calcined at 823 K for 8 h in air. The obtained Na-MOR was converted to NH_4-MOR through four sequential ion exchanges with a 1.0 M NH_4NO_3 aqueous solution at 353 K for 12 h.[4] The sample was dried at 383 K for 12 h and calcined at 773 K for 3 h in air, yielding HMOR. The Cu-HMOR catalyst was prepared by incipient impregnation, in which case 4.0 g of NH_4-MOR was suspended in 8 mL of 0.35 M $Cu(NO_3)_2$ aqueous solution at room temperature. After being allowed to dry at 383 K for 12 h, the resulting solid was calcined at 773 K in air for 3 h. To remove the external copper species, the sample was washed

Received: March 21, 2013
Revised: July 21, 2013
Accepted: July 29, 2013
Published: July 29, 2013

dx.doi.org/10.1021/ie400909u | *Ind. Eng. Chem. Res.* 2013, 52, 11510−11515

with a 0.05 M HNO_3 aqueous solution. The resulting solid was dried at 383 K for 12 h and calcined at 773 K for 3 h in air, giving the Cu-HMOR catalyst with a copper loading of 2.4 wt %, as measured by ICP analysis.

2.2. Characterization. X-ray diffraction (XRD) patterns of the samples were recorded on a D/MAX 2500 X-ray diffractometer (Rigaku) using Cu K_α radiation at 40 kV and 200 mA. N_2 adsorption isotherms were obtained at 77 K using a Quantachrome Autosorb-1-MP gas sorption analyzer. Before the measurements, each sample was degassed at 573 K for 2 h.

Field-emission scanning electron microscopy (FESEM) images were recorded using a Philips Fei Quanta 200F microscope operated at 20 kV. Samples were placed on a conductive carbon tape adhered to an aluminum sample holder. Transmission electron microscopy (TEM) images were recorded using an FEI Tecnai G2 Spirit microscope operated at 120 kV. The specimen was prepared by ultrasonically dispersing sample into ethanol and depositing droplets of the suspension on a carbon-enhanced copper grid and then dried in air.

Fourier transform infrared (FT-IR) spectra were recorded on a Bruker Vector-77 instrument at a resolution of 2 cm^{-1}. Before each measurement, the sample was evacuated at 723 K for 5 h.

Solid-state magic-angle-spinning (MAS) nuclear magnetic resonance NMR) experiments were carried out on a Varian Infinityplus-400 spectrometer. ^1H MAS NMR spectra were collected at 399.9 MHz with a 4-s recycle delay, 80 scans, and a spinning rate of 10 kHz. Chemical shifts were referenced to admantane. Spectral deconvolution was performed using the Dmfit software based on Gaussian−Lorentzian line shapes.[23]

Temperature-programmed desorption of ammonia (NH_3 TPD) experiments were conducted with a U-shape quartz tube reactor. For each experiment, a 100-mg sample was heated to 773 K at a rate of 10 K/min and maintained at this temperature for 1 h under He flow (30 mL/min). The sample was then purged with a 10 vol % NH_3/He mixture (30 mL/min) for 30 min at 473 K. The physically adsorbed ammonia was removed by purging the sample with a 0.6 vol % H_2O/He mixture (30 mL/min) at 473 K for 1 h.[9] After being allowed to cool to room temperature, the sample was heated to 873 K at a rate of 10 K/min under He flow (30 mL/min). The amount of NH_3 desorbed was monitored by mass spectrometry (Omnistar QMS200). Temperature-programmed oxidation (TPO) measurements of the used samples were conducted with the same instrument. Before the experiments, the sample (100 mg) was pretreated at 523 K for 1 h under He flow (40 mL/min). After being allowed to cool to room temperature, the sample was heated to 1073 K at a rate of 10 K/min in a flowing 20 vol % O_2/He mixture (40 mL/min). The effluent was monitored by mass spectrometer.

2.3. DME Carbonylation. DME carbonylation was tested in a continuous-flow fixed-bed microreactor with an inner diameter of 8 mm. For each experiment, 100 mg of sample (40−60 mesh) was loaded into the reactor, heated to 573 K at a rate of 3 K/min under the flow of a 20 vol % H_2/CO mixture (8.34 mL/min), and kept at that temperature for 3 h. The gas feed composition was then shifted to a mixture of DME, CO, H_2, and He in a ratio of $5/76/x/(19 - x)$ with x = 0, 5, and 19 vol % (8.34 mL/min), and the reactor was pressurized to 1.0 MPa. The effluent from the reactor was analyzed by an online gas chromatograph (Agilent 6890N) equipped with a thermal conductivity detector (TCD) and a flame ionization detector (FID).

3. RESULTS AND DISCUSSION

3.1. Textural and Chemical Properties of the Catalysts. Figure 1 shows XRD patterns of the samples.

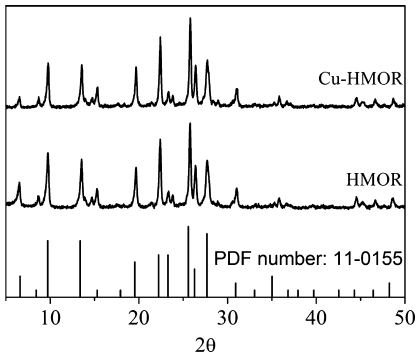

Figure 1. XRD patterns of HMOR and Cu-HMOR samples.

Typical diffraction lines of mordenite-type zeolites (PDF number 11-0155) were clearly observed for the two samples. Compared to the nanosized HMOR, the Cu-HMOR catalyst had a slightly decreased relative crystallinity but an increased surface area and pore volume (see Table 1), indicating that the acidic treatment during copper removal leached the extraframework alumina species in the channels.[24] Figure 2 shows FESEM/TEM images of the samples. The HMOR sample had a cubic morphology with sizes ranging from 50 to 100 nm, differing significantly from the traditional blocklike morphology with typical sizes of 2−6 μm.[9,10] The copper loading did not alter the morphology or size of the catalyst. TEM analysis did not reveal the presence of copper particles on the surface, implying that the copper species might exchange with the protons and locate inside the channels.

Table 1. Textural and Chemical Properties of the Catalysts

sample	S_{BET} (m^2/g)	S_{micro} (m^2/g)	V_{total} (mL/g)	V_{micro} (mL/g)
HMOR	567	484	0.806	0.195
Cu-HMOR	589	515	0.761	0.202
	NH_3 desorption amount (mmol/g)			
	total	8-MR	12-MR	
HMOR	0.69	0.45	0.24	
Cu-HMOR	0.31	0.20	0.11	

Figure 3a shows the IR spectra of the HMOR and Cu-HMOR samples. The band at 3744 cm^{-1} is usually assigned to the −SiOH stretching vibration. The band at 3610 cm^{-1} for acidic bridging −OH stretching vibration was actually the combination of the bands for two types of acid sites in the 12-MR channels (~3612 cm^{-1}) and the 8-MR channels (~3590 cm^{-1}).[4,25,26] It is obvious that the band at 3610 cm^{-1} of the Cu-HMOR sample decreased significantly in comparison with that of the HMOR sample, indicating that the acidic bridging −OH groups might be exchanged by Cu ions.[27] Figure 3b shows the ^1H MAS NMR spectra of the HMOR and Cu-HMOR samples. The peak at 1.84 ppm was attributed to the isolated Si−OH on the crystallite surface and defect sites, whereas the peaks at about 2.76, 4.12, and 4.91 ppm are assigned to Al−OH group, Brønsted acidic site, and adsorbed water,[28−33] respectively. The Si/Al ratio in the HMOR sample was about 22. For the Cu-HMOR sample, the intensity of the peak at 4.12 ppm decreased

dx.doi.org/10.1021/ie400909u | Ind. Eng. Chem. Res. 2013, 52, 11510−11515

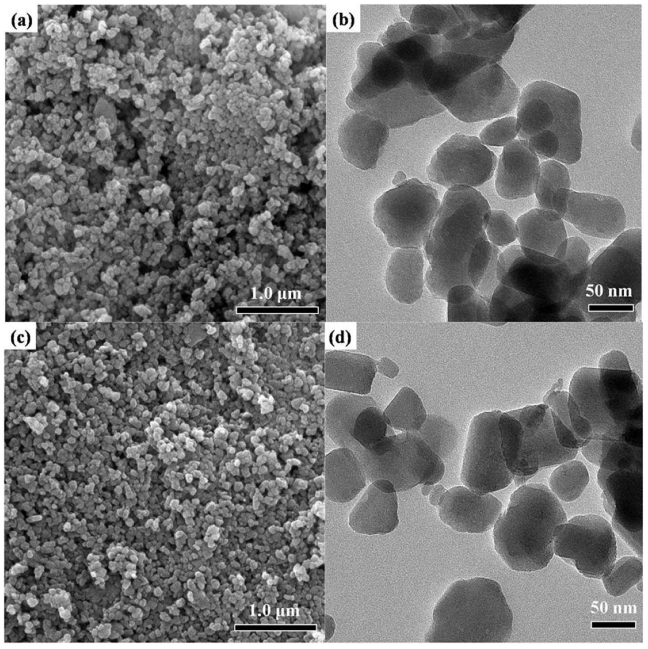

Figure 2. FESEM and TEM images of (a,b) HMOR and (c,d) Cu-HMOR samples.

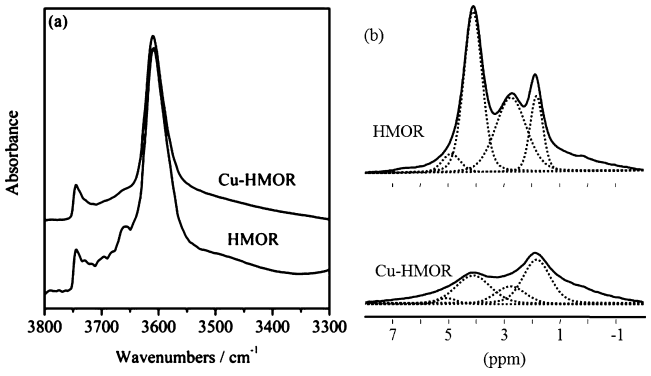

Figure 3. (a) FT-IR and (b) ^{1}H MAS NMR spectra of HMOR and Cu-HMOR samples.

considerably, probably because of the substitution of the Brønsted acidic sites by copper cation. From the ^{1}H MAS NMR measurements, it was estimated that about 55% of the Brønsted acidic sites were removed upon the addition of 2.4 wt % copper. Figure 4 shows the NH_3 TPD profiles of the samples. Two distinct ammonia desorptions at 460 and 810 K appeared on the HMOR sample, corresponding to weak and strong acidic sites, respectively. The weakly adsorbed ammonia was effectively removed by water vapor at about 473 K, facilitating the quantitative determination of the strong Brønsted acidic sites.[9,34,35] Because the kinetic diameter of the pyridine molecule (0.585 nm) is much larger than that of the 8-MR channels but very close to the pore size of the 12-MR channels, preadsorption of pyridine at 573 K selectively poisoned the acidic sites in the 12-MR channels, and accordingly, the amount of Brønsted acid sites in the 8-MR channels was estimated.[9] The HMOR sample had a total amount of Brønsted acidic sites of 0.69 mmol/g, comprising 0.45 mmol/g in the 8-MR channels and 0.24 mmol/g in the 12-MR channels. For the Cu-HMOR sample, an additional desorption peak at about 600 K was observed, resulting from

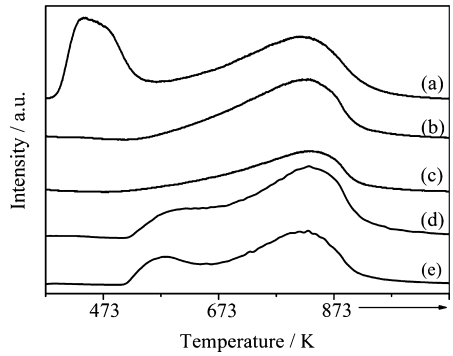

Figure 4. NH_3 TPD profiles of (a−c) HMOR (a) before and (b) after water treatment and (c) after pyridine adsorption and (d,e) Cu-HMOR (d) without and (e) with pyridine adsorption.

the decomposition of a copper ammonia complex that was formed during ammonia adsorption.[36,37] Together with the ^{1}H MAS NMR result in Figure 3, the total amount of the Brønsted acidic sites on the Cu-HMOR catalyst was estimated to be 0.31 mmol/g: 0.20 mmol/g in the 8-MR channels and 0.11 mmol/g in the 12-MR channels. These results further demonstrate that the copper cations were almost equally exchanged with the protons in both 8-MR and 12-MR channels.

3.2. DME Carbonylation. Figure 5a compares the conversion of DME and the product selectivity during DME carbonylation over the HMOR-C, HMOR, and Cu-HMOR catalysts at 573 K. On the microsized HMOR-C catalyst, the conversion of DME was about 69% at the initial stage, but it decreased sharply to about 20% at 2 h and then gradually decreased to only 3% at 9 h, showing a rapid deactivation pattern. Over the nanosized HMOR catalyst, the conversion of DME initially approached almost 100%, with aromatics (mostly alkylbenzenes) and light olefins (ethylene, propylene, and butene) being produced as the major products. The selectivity of olefins rapidly decreased from 24% at the very beginning to 4% at 4 h, and the selectivity of aromatics decreased from 75% to 55% at 4 h, whereas the selectivity of MA gradually increased to about 40% at 4 h. This reaction pattern confirms that the formation of aromatics through olefins during the induction period of about 4 h was the dominant reaction, mainly occurring within the 12-MR channels.[5,11] With the accumulation of aromatics in the 12-MR channels, DME carbonylation in the 8-MR channels became the major reaction after the induction period. During the subsequent reaction period of 4−10 h, an apparent deactivation was observed. The conversion of DME decreased from about 100% to about 65%, and the selectivity of aromatics decreased to 30%, whereas the selectivity of MA increased to about 70%. This product distribution indicates that the formation of MA in the 8-MR channels was linked with the production of aromatics in the 12-MR channels. Thereafter, the reaction experienced a relatively slow deactivation process. After 40 h, the conversion of DME decreased gradually to about 20%, and the selectivity of aromatics declined to 10%, whereas the selectivity of MA gradually increased to 88%. On the Cu-HMOR catalyst, however, the reaction pattern was altered considerably. The induction period was shortened to only about 2 h, and the catalyst stability was promoted significantly. At the very beginning of the reaction, substantial amounts of aromatics were readily produced with a selectivity of 75%. After 2 h, the selectivity of aromatics decreased sharply to about 34%,

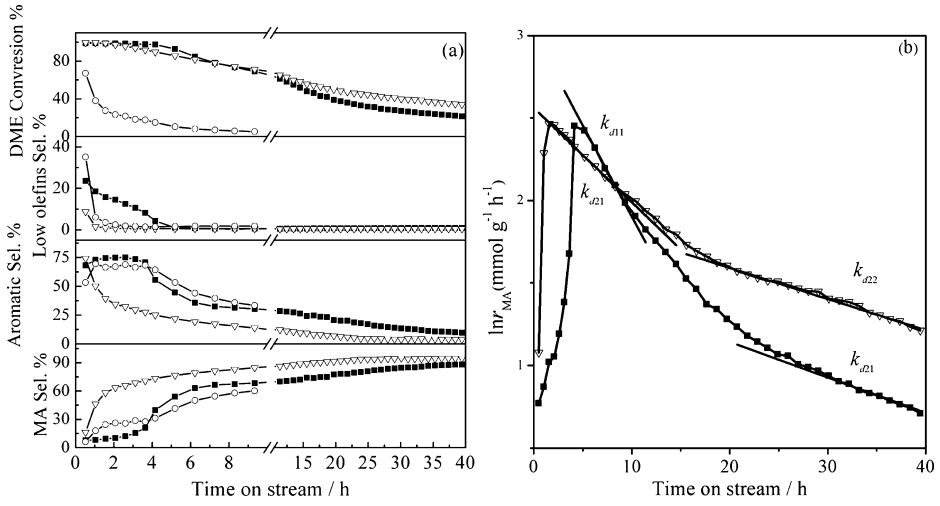

Figure 5. (a) DME conversion and product selectivity and (b) deactivation patterns on (○) HMOR-C, (■) HMOR, and (▽) Cu-HMOR catalysts during DME carbonylation. Reaction conditions: 573 K, 1 MPa, 5 vol % DME/76 vol % CO/19 vol % He, 5000 mL/g·h.

whereas the selectivity of MA increased rapidly to 64%. This result indicates that copper within the HMOR channels activated CO and expedited DME carbonylation effectively, in agreement with the previous observation that the presence of copper in HMOR not only activated CO but also adsorbed DME preferentially.[2] Thereafter, the selectivity of aromatics decreased to 4%, whereas the selectivity of MA gradually increased to 94% at 40 h.

Figure 5b compares the deactivation rate constants (k_d) of DME carbonylation on the HMOR and Cu-HMOR catalysts. There were two distinct deactivation regions: The fast deactivation occurred just after the induction period as a result of the heavy deposition of coke mostly on the Brønsted acidic sites, whereas the slow deactivation lasted for a long period with a gradual buildup of carbonaceous species on the catalyst surface.[38] k_{d1} and k_{d2}, which refer to the rate constants of the rapid and slow deactivations, respectively, were derived from the production rates of MA using the power-law equation

$$-r_d = -da/dt = k_d a^d$$

where r_d is the deactivation rate, a is the relative activity of catalyst at time t (h), and d is the order of deactivation.[39−41] For the HMOR catalyst, the fast deactivation rate constant, k_{d1}, was 0.10 h^{-1}, whereas it was only 0.053 h^{-1} for the Cu-HMOR catalyst. Notably, these deactivation rates correlate well with the number of Brønsted acidic sites located within the 12-MR channels of the samples. However, there was no apparent difference in the slow deactivation rate constants for the two samples, being about 0.020 h^{-1} in both cases.

Figure 6 compares the TPO profiles of the coked catalysts at different intervals. On the coked HMOR catalyst, desorption of carbon oxides occurred at 530−950 K with the presence of at least three types of coke species. Specifically, the desorption peak at about 650 K was likely due to the combustion of soft coke, surface-bound methyl and acetyl species associated with the formation of MA. The desorption peaks at 800−880 K can be ascribed to the combustion of hard coke.[9,10,42,43] Quantitative analyses indicated that substantial amounts of both soft and hard cokes were immediately formed at the very beginning of the reaction and approached 102.6 mg of C/g at 4 h. Thereafter, the amount of coke increased slightly to 122.3 mg of C/g at 14 h and to 138.0 mg of C/g at 40 h, including

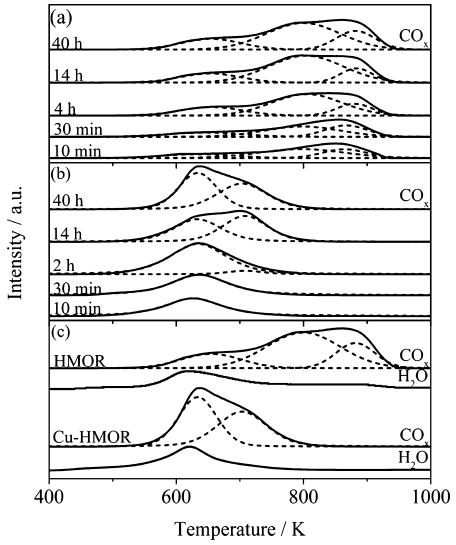

Figure 6. TPO profiles of the coked catalysts at different intervals during DME carbonylation: (a) HMOR, (b) Cu-HMOR, and (c) the samples after reaction for 40 h.

19% soft coke and 81% hard coke. This coking behavior indicates that heavy coke deposition occurred mainly in the induction period. In contrast, the coking behavior on the Cu-HMOR catalyst was quite different. There was only a low-temperature desorption peak at about 630 K at the initial stage of the reaction, representing the soft coke. The amount of the soft coke was 47.1 mg of C/g at 10 min and increased to 85.7 mg of C/g at 2 h. Thereafter, a new desorption peak of carbon oxides appeared at 705 K, indicating the formation of another type of coke that gradually increased over time. The total amount of coke increased slightly to 118.1 mg of C/g at 40 h, containing 51% soft coke and 49% hard coke. Compared with that on the HMOR catalyst, the amount of soft coke on the Cu-HMOR catalyst was relatively higher, probably resulting from copper activation. Unlike for the HMOR catalyst, the CO_2 desorption peak above 800 K did not appear for the Cu-HMOR catalyst. This confirms that the copper species almost completely suppressed the formation of hard coke. To distinguish the chemical natures of these cokes, TPO

dx.doi.org/10.1021/ie400909u | Ind. Eng. Chem. Res. 2013, 52, 11510−11515

measurements of the coked samples at the end of the runs was further investigated by comparing CO_x and H_2O evolutions as shown in Figure 6c. The simultaneous formation of CO_x and water at 630−650 K indicated a higher H/C ratio in the soft cokes that can presumably be assigned to surface-bound methyl and acetyl species,[38,42,44,45] but the high-temperature desorption peaks at 800−880 K on the HMOR catalyst and at 705 K on the Cu-HMOR catalyst had a much lower mole ratio of H/C, indicating the combustion of hard cokes.

3.3. H_2 Promotion Effect. Addition of a small amount of H_2 to the feed stream has been demonstrated to be effective in suppressing coke formation on zeolites at high temperatures.[46,47] Compared with the reaction results shown in Figure 5, hydrogen addition to the reaction gas was found to markedly promote the activity and stability on both catalysts. As illustrated in Figure 7, on the HMOR catalyst, as the hydrogen concentration in the feed gas was increased from 5 to 19 vol %, the induction period was obviously extended to about 8 h, the selectivity of aromatics increased from 17% to 23% at 40 h, and the selectivity of MA decreased slightly from 80% to 75%. Taking the conversion of DME into account, the formation rate of MA increased from 3.1 to 5.3 mmol/g·h as the H_2 concentration increased from 5 to 19 vol %, confirming the promoting effect of hydrogen in DME carbonylation. This phenomenon was more significant on the Cu-HMOR catalyst. The formation rate of MA increased from 6.5 mmol/g·h at 5 vol % H_2 to 8.6 mmol/g·h at 19 vol % H_2. Therefore, the activity and the stability were promoted considerably by hydrogen addition to the Cu-HMOR catalysts.

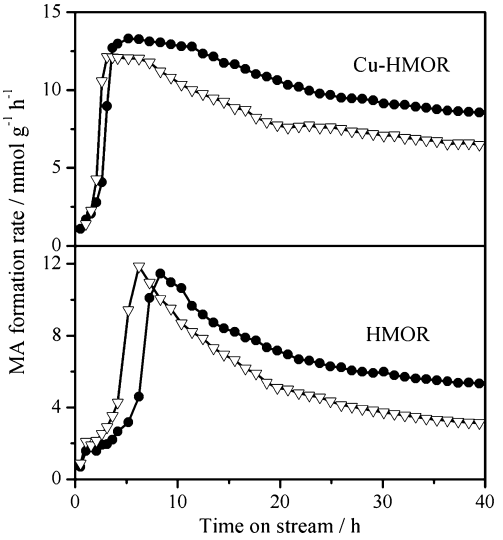

Figure 7. MA formation rates on HMOR and Cu-HMOR catalysts with the addition of (▽) 5 and (●) 19 vol % H_2 to the feed gas. Reaction conditions: 5 vol % DME/76 vol % CO/19 vol % (H_2 + He), 5000 mL/g·h, 573 K, and 1.0 MPa.

Table 2 summarizes the amounts of coke deposited and the deactivation rate constants (k_{d1} and k_{d2}) with H_2 addition to the feed gas. Both k_{d1} and k_{d2} decreased obviously as the amount of H_2 increased, implying that the deactivation was suppressed upon H_2 addition. Moreover, as the hydrogen concentration in the feed gas increased from 5 to 19 vol %, the amounts of hard cokes that formed after the induction periods on both catalysts were effectively suppressed, evidencing the positive role of hydrogen in coke elimination under the reaction conditions investigated.

Table 2. Deactivation Rate Constants and Coke Amounts

H_2 (vol %)	deactivation rate constant (h^{-1})		coke formed at different intervals (mg of C/g)				
	k_{d1}	k_{d2}	10 min	40 min	2 or 4 h[a]	14 h	40 h
			HMOR				
—	0.10	0.023	58.3	66.5	102.6	122.3	138.0
5	0.069	0.015	—	—	108.1	—	119.8
19	0.049	0.011	—	—	100.8	—	102.0
			Cu-HMOR				
—	0.053	0.020	47.1	55.6	85.7	101.6	118.1
5	0.038	0.011	—	—	86.9	—	102.0
19	0.023	0.009	—	—	87.0	—	94.8

[a]Induction periods were 4 and 2 h for the HMOR and Cu-HMOR catalysts, respectively.

4. CONCLUSIONS

Nanosized HMOR showed significantly enhanced activity and stability in the DME carbonylation reaction, compared to conventional microsized mordenite. Copper incorporation into the channels further promoted the overall reaction efficiency and lowered the deactivation rates based on the fact that copper activated CO under reaction conditions and simultaneously eliminated the accumulation of hard coke. Furthermore, addition of hydrogen to the feed gas was also effective in suppressing coke formation, and this promotion effect was more significant on the Cu-HMOR catalyst. As a consequence, the production rate of methyl acetate approached 9 mmol/g·h after 40 h at 573 K.

AUTHOR INFORMATION

Corresponding Author

*E-mail: shen98@dicp.ac.cn.

Notes

The authors declare no competing financial interest.

ACKNOWLEDGMENTS

We acknowledge financial support for this research from the National Basic Research Program of China (2013CB933100), the National Natural Science Foundation of China (20973166), and BP Chemicals Limited.

REFERENCES

(1) Cheung, P.; Bhan, A.; Sunley, G. J.; Iglesia, E. Selective Carbonylation of Dimethyl Ether to Methyl Acetate Catalyzed by Acidic Zeolites. *Angew. Chem., Int. Ed.* **2006**, *45*, 1617.

(2) Blasco, T.; Boronat, M.; Concepción, P.; Corma, A.; Law, D.; Vidal-Moya, J. A. Carbonylation of Methanol on Metal−Acid Zeolites: Evidence for a Mechanism Involving a Multisite Active Center. *Angew. Chem., Int. Ed.* **2007**, *46*, 3938.

(3) Cheung, P.; Bhan, A.; Sunley, G. J.; Law, D. J.; Iglesia, E. Site Requirements and Elementary Steps in Dimethyl Ether Carbonylation Catalyzed by Acidic Zeolites. *J. Catal.* **2007**, *245*, 110.

(4) Bhan, A.; Allian, A. D.; Sunley, G. J.; Law, D. J.; Iglesia, E. Specificity of Sites within Eight-Membered Ring Zeolite Channels for Carbonylation of Methyls to Acetyls. *J. Am. Chem. Soc.* **2007**, *129*, 4919.

(5) Boronat, M.; Martinez-Sanchez, C.; Law, D.; Corma, A. Enzyme-like Specificity in Zeolites: A Unique Site Position in Mordenite for

Selective Carbonylation of Methanol and Dimethyl Ether with CO. *J. Am. Chem. Soc.* **2008**, *130*, 16316.
(6) Armitage, G. G.; Sunley, J. G. Selective Dealumination of MOR Type Zeolites. European Patent EP2174713 A1, 2010.
(7) Ditzel, E. J.; Law, D. J.; Sunley, J. G. Carbonylation Process Using Bound Silver and/or Copper Mordenite Catalysts. World Patent WO2010067043 A1, 2010.
(8) Ditzel, E. J.; Law, D. J.; Roberts, M. S. Process for the Carbonylation of Dimethyl Ether. U.S. Patent Application 2010/0130771 A1. 2010.
(9) Liu, J. L.; Xue, H. F.; Huang, X. M.; Wu, P. H.; Huang, S. J.; Liu, S. B.; Shen, W. J. Stability Enhancement of H-Mordenite in Dimethyl Ether Carbonylation to Methyl Acetate by Pre-adsorption of Pyridine. *Chin. J. Catal.* **2010**, *31*, 729.
(10) Liu, J. L.; Xue, H. F.; Huang, X. M.; Li, Y.; Shen, W. J. Dimethyl Ether Carbonylation to Methyl Acetate over HZSM-35. *Catal. Lett.* **2010**, *139*, 33.
(11) Boronat, M.; Martinez, C.; Corma, A. Mechanistic Differences between Methanol and Dimethyl Ether Carbonylation in Side Pockets and Large Channels of Mordenite. *Phys. Chem. Chem. Phys.* **2011**, *13*, 2603.
(12) Guisnet, M.; Costa, L.; Ribeiro, F. R. Prevention of Zeolite Deactivation by Coking. *J. Mol. Catal. A.* **2009**, *305*, 69.
(13) Mochizuki, H.; Yokoi, T.; Imai, H.; Watanabe, R.; Namba, S.; Kondo, J. N.; Tatsumi, T. Facile Control of Crystallite Size of ZSM-5 Catalyst for Cracking of Hexane. *Microporous Mesoporous Mater.* **2011**, *145*, 165.
(14) Rownaghi, A. A.; Rezaei, F.; Hedlund, J. Selective Formation of Light Olefin by *n*-Hexane Cracking over HZSM-5: Influence of Crystal Size and Acid Sites of Nano- and Micrometer-Sized Crystals. *Chem. Eng. J.* **2012**, *191*, 528.
(15) Tago, T.; Konno, H.; Sakamoto, M.; Nakasaka, Y.; Masuda, T. Selective Synthesis for Light Olefins from Acetone over ZSM-5 Zeolites with Nano- and Macro-Crystal Sizes. *Appl. Catal. A* **2011**, *403*, 183.
(16) Tago, T.; Konno, H.; Nakasaka, Y.; Masuda, T. Size-Controlled Synthesis of Nano-Zeolites and Their Application to Light Olefin Synthesis. *Catal. Surv. Asia.* **2012**, *16*, 148.
(17) Choi, M.; Na, K.; Kim, J.; Sakamoto, Y.; Terasaki, O.; Ryoo, R. Stable Single-Unit-Cell Nanosheets of Zeolite MFI as Active and Long-Lived Catalysts. *Nature* **2009**, *461*, 246.
(18) Jang, H.-G.; Min, H.-K.; Lee, J. K.; Hong, S. B.; Seo, G. SAPO-34 and ZSM-5 Nanocrystals' Size Effects on Their Catalysis of Methanol-to-Olefin Reactions. *Appl. Catal. A* **2012**, *437*, 120.
(19) Rownaghi, A. A.; Rezaei, F.; Stante, M.; Hedlund, J. Selective Dehydration of Methanol to Dimethyl Ether on ZSM-5 Nanocrystals. *Appl. Catal. B* **2012**, *119*, 56.
(20) Ji, X.; Qin, Z.; Dong, M.; Wang, G.; Dou, T.; Wang, J. Friedel–Crafts Acylation of Anisole and Toluene with Acetic Anhydride over Nano-Sized Beta Zeolites. *Catal. Lett.* **2007**, *117*, 171.
(21) Xue, H. F.; Huang, X. M.; Evert, D.; Zhan, E. S.; Ma, M.; Shen, W. J. Coking on Micrometer- and Nanometer-Sized Mordenite during Dimethyl Ether Carbonylation to Methyl Acetate. *Chin. J. Catal.* **2013**, *34*, 1496.
(22) Lee, S. H.; Lee, D. K.; Shin, C. H.; Paik, W. C.; Lee, W. M.; Hong, S. B. Synthesis of Zeolite ZSM-57 and Its Catalytic Evaluation for the 1-Butene Skeletal Isomerization and *n*-Octane Cracking. *J. Catal.* **2000**, *196*, 158.
(23) Massiot, D.; Fayon, F.; Capron, M.; King, I.; Le Calve, S.; Alonso, B.; Durand, J. O.; Bujoli, B.; Gan, Z. H.; Hoatson, G. Modelling One- and Two-Dimensional Solid-State NMR Spectra. *Magn. Reson. Chem.* **2002**, *40*, 70.
(24) Meyers, B. L.; Fleisch, T. H.; Ray, G. J.; Miller, J. T.; Hall, J. B. A Multitechnique Characterization of Dealuminated Mordenites. *J. Catal.* **1988**, *110*, 82.
(25) Zholobenko, V. L.; Makarova, M. A.; Dwyer, J. Inhomogeneity of Bronsted Acid Sites in H-Mordenite. *J. Phys. Chem.* **1993**, *97*, 5962.
(26) Maache, M.; Janin, A.; Lavalley, J. C.; Benazzi, E. FT Infrared Study of Bronsted Acidity of H-Mordenites: Heterogeneity and Effect of Dealumination. *Zeolites* **1995**, *15*, 507.
(27) Montanari, T.; Bevilacqua, M.; Resini, C.; Busca, G.; Pirone, R.; Ruoppolo, G. A Spectroscopic Study of the Nature and Accessibility of Protonic and Cationic Sites in H- and Partially Exchanged Cu- and Co-MFI Zeolites. *J. Porous Mater.* **2007**, *14*, 291.
(28) Freude, D.; Hunger, M.; Pfeifer, H. Study of Bronsted Acidity of Zeolites Using High-Resolution Proton Magnetic-Resonance with Magic-Angle Spinning. *Chem. Phys. Lett.* **1982**, *91*, 307.
(29) Freude, D.; Hunger, M.; Pfeifer, H.; Schwieger, W. ^{1}H Mas NMR Studies on the Acidity of Zeolites. *Chem. Phys. Lett.* **1986**, *128*, 62.
(30) Klinowski, J. Solid-State NMR Studies of Molecular-Sieve Catalysts. *Chem. Rev.* **1991**, *91*, 1459.
(31) Hunger, M.; Freude, D.; Pfeifer, H. Magic-Angle Spinning Nuclear Magnetic Resonance Studies of Water Molecules Adsorbed on Brønsted- and Lewis-Acid Sites in Zeolites and Amorphous Silica–Aluminas. *J. Chem. Soc., Faraday. Trans.* **1991**, *87*, 657.
(32) Deng, F.; Du, Y. R.; Ye, C. H.; Wang, J. Z.; Ding, T. T.; Li, H. X. Acid Sites and Hydration Behavior of Dealuminated Zeolite HZSM-5: A High-Resolution Solid-State NMR Study. *J. Phys. Chem.* **1995**, *99*, 15208.
(33) Hayashi, S.; Kojima, N. Acid Properties of H-type Mordenite Studied by Solid-State NMR. *Microporous Mesoporous Mater.* **2011**, *141*, 49.
(34) Bagnasco, G. Improving the Selectivity of NH_3 TPD Measurements. *J. Catal.* **1996**, *159*, 249.
(35) Katada, N.; Niwa, M. Analysis of Acidic Properties of Zeolitic and Non-Zeolitic Solid Acid Catalysts Using Temperature-Programmed Desorption of Ammonia. *Catal. Surv. Asia.* **2004**, *8*, 161.
(36) Salker, A. V.; Weisweiler, W. Catalytic Behaviour of Metal Based ZSM-5 Catalysts for NO_x Reduction with NH_3 in Dry and Humid Conditions. *Appl. Catal. A* **2000**, *203*, 221.
(37) Putluru, S. S. R.; Riisager, A.; Fehrmann, R. Alkali Resistant Cu/Zeolite deNO_x Catalysts for Flue Gas Cleaning in Biomass Fired Applications. *Appl. Catal. B* **2011**, *101*, 183.
(38) Kam, E. K. T.; Al-Shamali, M.; Juraidan, M.; Qabazard, H. A Hydroprocessing Multicatalyst Deactivation and Reactor Performance Model-Pilot-Plant Life Test Applications. *Energy Fuels* **2005**, *19*, 753.
(39) Levenspi., O. Experimental Search for a Simple Rate Equation to Describe Deactivating Porous Catalyst Particles. *J. Catal.* **1972**, *25*, 265.
(40) Levenspiel, O. The Coming-of-Age of Chemical-Reaction Engineering. *Chem. Eng. Sci.* **1980**, *35*, 1821.
(41) Yao, S.; Gu, L.; Sun, C.; Li, J.; Shen, W. Combined Methane CO_2 Reforming and Dehydroaromatization for Enhancing the Catalyst Stability. *Ind. Eng. Chem. Res.* **2009**, *48*, 713.
(42) Guisnet, M.; Magnoux, P. Organic Chemistry of Coke Formation. *Appl. Catal. A* **2001**, *212*, 83.
(43) Palumbo, L.; Bonino, F.; Beato, P.; Bjorgen, M.; Zecchina, A.; Bordiga, S. Conversion of Methanol to Hydrocarbons: Spectroscopic Characterization of Carbonaceous Species Formed over H-ZSM-5. *J. Phys. Chem. C.* **2008**, *112*, 9710.
(44) Kim, S. J.; Park, J. W.; Lee, K. Y.; Seo, G.; Song, M. K.; Jeong, S.-Y. Enhanced Catalytic Performance of Copper-Exchanged SAPO-34 Molecular Sieve in Methanol-to-Olefin Reaction. *J. Nanosci. Nanotechnol.* **2010**, *10*, 147.
(45) Cai, W.; Wang, F.; Daniel, C.; van Veen, A. C.; Schuurman, Y.; Descorme, C.; Provendier, H.; Shen, W.; Mirodatos, C. Oxidative Steam Reforming of Ethanol over Ir/CeO_2 Catalysts: A Structure Sensitivity Analysis. *J. Catal.* **2012**, *286*, 137.
(46) Liu, Z.; Nutt, M. A.; Iglesia, E. The Effects of CO_2, CO and H_2 Co-reactants on Methane Reactions Catalyzed by Mo/H-ZSM-5. *Catal. Lett.* **2002**, *81*, 271.
(47) Shu, Y. Y.; Ma, H. T.; Ohnishi, R.; Ichikawa, M. Highly Stable Performance of Catalytic Methane Dehydrocondensation towards Benzene on Mo/HZSM-5 by a Periodic Switching Treatment with H_2 and CO_2. *Chem. Commun.* **2003**, *39*, 86.